

**USING UNMANNED AERIAL SYSTEMS TO CLASSIFY LAND COVER AND ASSESS  
PRODUCTIVITY IN FORESTED WETLANDS IN NOVA SCOTIA**

by

Iain M.J.C. Wilson

A thesis submitted in fulfillment of the

requirements of BEST 4599

for the Degree of Bachelor of Environmental Studies (Honours)

Bachelor of Environmental Studies Program

Saint Mary's University

Halifax, Nova Scotia, Canada

© I. M. Wilson, 2019

April 12, 2019

Members of the Examining Committee:

Dr. Karen Harper (Supervisor)

Department of Geography and Environmental Studies

Saint Mary's University

Dr. Danika Van Proosdij

Department of Geography and Environmental Studies

Saint Mary's University

## **ABSTRACT**

### **Using Unmanned Aerial Systems to Classify Land Cover and Assess Productivity in Forested Wetlands in Nova Scotia**

by

Iain M.J.C. Wilson

Forested wetlands in Nova Scotia are an understudied and ephemeral ecosystem type with high predicted ecological value. They are thought to cover a broad geographical area; however, their distribution is difficult to quantify, partly due to their similarity to drier forested landscapes in ordinary RGB aerial imagery. This study used unmanned aerial systems (UAS) imagery to attempt to classify and quantify the distribution of forested wetland communities, differentiate forested wetlands from drier forested communities, and assess productivity levels using the normalized difference vegetation index (NDVI). This study is one of the first known examples of UAS use in forested wetland ecosystems. NDVI imagery was captured in the Musquodoboit River valley during the summer of 2018 using a consumer-grade UAS and processed into orthomosaic maps in Pix4D Mapper Pro. The maximum likelihood classifier algorithm was applied to the dataset to group similar pixels into land cover classes based on ground truth data collected in the same time frame as the UAS flights. The classification scheme was then put through a confusion matrix to assess its accuracy. Based on this assessment, the classification was not accurate. This may be due to several factors, including flaws in the ground sampling method, and the fact that forests are generally difficult to classify through pixel-based classification methods. NDVI values did not differ greatly across land cover classes, which may have played a role in the unsuccessful classification. Suggestions for future studies include using a more rigorous and quantitative ground sampling protocol and considering different classification methods, such as object-based image analysis (OBIA).

April 12, 2019

## **ACKNOWLEDGEMENTS**

I owe thanks to so many people and organizations for making this project happen and supporting me along the way. First and foremost, I must extend my sincerest gratitude to my supervisor, Dr. Karen Harper, for her constant support and advice when the going got tough (as it quite often did), and for affording me the opportunity to take on a research project of my own and to work in the field of environmental science. The experience was invaluable and has helped me grow as a student, as a writer, and as a person in general. I must also mention the support of Dr. Danika Van Proosdij, who was gracious enough to lend some of her very limited spare time to this project as a second reader and offer advice and feedback on the project, especially during the early stages. Her experience with similar projects was crucial to developing the framework of this study. Next, I thank Greg Baker at the Maritime Provinces Spatial Analysis and Research Centre for his incredible assistance throughout the duration of this project. Greg is a true treasure at SMU and was always cheerful and eager to help me out with the more technical aspects of this endeavor that were often well out of my range of knowledge. He was also responsible for organizing and providing equipment rentals and data processing workspace, without which this study never could have been carried out. I also recognize my colleagues in the field over the summer, Morgan Rice and Georgia Konstantanidis, who assisted with data collection and site preparation. Many thanks to both of them for their hard work and upbeat attitudes. This project was undertaken with the financial support of the Government of Canada as part of the Biodiversity and Ecosystem Functioning of Forested Wetlands Across Atlantic Canada project. Additional funding was provided by NSERC, Saint Mary's University, Dalhousie University, Nova Scotia Labour and Advanced Education Co-op Education Incentive Application, and Project Learning Tree Canada.

## TABLE OF CONTENTS

Abstract .....	i
Acknowledgements .....	ii
List of Tables .....	iv
List of Figures .....	v
Chapter 1    Introduction.....	1
Chapter 2    Methods .....	8
Chapter 3    Results .....	23
Chapter 4    Discussion, and Recommendations.....	32
List of References.....	41
Appendix.....	47

## LIST OF TABLES

Table 1	Land cover class criteria.....	15
Table 2	Confusion matrix for flight day 1.....	31
Table 3	Confusion matrix for flight day 2.....	32

## LIST OF FIGURES

Figure 1	Study area at Gates 1 Nature Preserve.....	11
Figure 2	Ground control points at Gates 1 Nature Preserve.....	13
Figure 3	Ground truth plots at Gates 1 Nature Preserve.....	14
Figure 4	Number of overlapping images computed for each pixel of the orthomosaic for flight day 1 (left) and flight day 2 (right).....	24
Figure 5	Computed image positions with links between matched images for flight day 1 (a) and flight day 2 (b).....	25
Figure 6	NDVI values from flight day 1 (a) and flight day 2 (b) at Gates 1 Nature Preserve.....	27
Figure 7	Mean NDVI values from flight day 1 (a) and flight day 2 (b).....	28
Figure 8	Classification of ecosystems from flight day 1 (a) and flight day 2 (b) at Gates 1 Nature Preserve.....	29

Figure A 1 Ground truth plot vegetation data.....47

Figure A 2 Pix4D Mapper Pro quality report summary for flight day 1 (a) and flight day 2  
(b).....49

Figure A 3 Pixel value histograms for NDVI maps from flight day 1 (a) and flight day 2  
(b).....50

## CHAPTER 1: Introduction

### 1. Introduction

In general, forested wetlands are an understudied ecosystem type due to their ephemeral and complex structure. Forested wetlands exist ubiquitously across Nova Scotia, but their distribution and extent are not well quantified (Brazner and Achenbach, n.d.). This may be because forested wetlands are generally indistinguishable from forested upland in typical aerial RGB imagery. However, differences in net primary productivity (NPP) between forested wetlands and forested uplands may help to discern their distribution through vegetation indices that employ non-visible bands of the electromagnetic spectrum, such as the normalized difference vegetation index (NDVI). Cronk and Fennessy (2009) note that productivity in wetlands varies from high levels ( $>2500 \text{ g/m}^2/\text{y}$ ) to lower levels in colder climates ( $100 \text{ g/m}^2/\text{y}$ ), while forested landscapes generally are moderately productive ( $800 \text{ g/m}^2/\text{y}$ ). If these differences are detectable through remotely-sensed NDVI imagery, forested wetlands may be more easily inventoried and quantified.

Unmanned aerial systems (UAS) represent a low-cost, user-friendly means of collecting high resolution multi-spectral data from forested wetlands compared to other remote sensing methods, such as LiDAR and satellite imagery. UAS studies in forested landscapes in general are sparse, and especially in forested wetland landscapes. Thus, one of the purposes of this study is to investigate the usability of UAS in forested wetland ecosystems.

The three main questions that this study seeks to answer are: 1) can differences in NPP be used to discriminate between forested uplands and forested wetlands?; 2) can existing UAS-based land classification techniques be used to classify forested wetland types?; and 3) do NDVI

values differ significantly between types of forested wetlands? Thus, the three main objectives of this study are: 1) classify an open wetland-forested wetland-forested upland mosaic landscape using NDVI maps derived from UAS imagery; 2) assess primary productivity in forested wetlands through the same NDVI maps; and 3) assess the effectiveness of UAS technologies in forested wetland landscapes. In relation to these questions, it is hypothesised that NDVI will differ significantly between forested wetland types. In addition, it is predicted that classification methods will succeed in classifying forested wetlands.

### **1.1 Remote sensing**

Remote sensing has existed for several decades and has allowed humans to observe the world in revolutionary ways. As technology has progressed, remote sensing has become more and more accurate, and thus more and more integral to the study of the planet and its processes. Remote sensing as we know it today has existed since the 1950's with the launch of the first Earth-observing satellites (Khorram et al., 2012). However, the general definition of remote sensing covers much more than just observing Earth's surface. Khorram et al., 2012 define remote sensing as "...the acquisition and measurement of information about certain properties of phenomena, objects, or materials by a recording device not in physical contact with the features under surveillance." Khorram et al. (2012) go on to note that this definition consequently includes things such as medical technologies, like X-ray and magnetic resonance imaging (MRI). To narrow this definition down to an environmental context, Khorram et al. (2012) specify that remote sensing of the environment is specifically measuring levels of electromagnetic radiation that emanates from areas or objects on (or in) Earth's surface, in its oceans, or in its atmosphere. Differences in the levels of electromagnetic radiation that is emanated from different surfaces

and objects allow different areas and objects to be discriminated from one another. This is the core concept of remote sensing in this context.

## **1.2 UAS**

In recent years, UAS have proliferated significantly through geospatial sciences in a myriad of applications, including coastal geomorphology monitoring (Clark, 2017), invasive species mapping (Michez et al., 2016a), classification and health assessment of vegetation (Michez et al., 2016b), and forest inventory (Puliti et al., 2015). These wide and varied uses are largely the result of the relatively low cost and simple operation of UAS platforms compared to other platforms that collect similar data, such as LiDAR and manned aircraft imagery. In addition, UAS are capable of capturing data at spatial and temporal scales that were previously impossible with established remote sensing methods. For example, Michez et al. (2016b) recently utilized high-resolution multi-temporal UAS imagery to classify and assess vegetation health in riparian forests with a high rate of success. The authors credit the ability of UAS methodology to capture events at very local scales and in finite time-frames as a major step forward in environmental science and ecology (Michez et al., 2016b). Similarly, Kuželka and Surový (2018) were able to use off-the-shelf consumer grade UAS to successfully create a 3D model of forest structure for use in sustainable forestry. This further confirms the versatility of UAS and speaks to the ever-increasing accuracy of these tools.

Several studies have sought to assess the spatial accuracy of UAS data in relation to more well-established techniques of describing Earth's surface, such as differential global positioning systems (DGPS). Lucier and Harwin (2012) found that high degrees of accuracy could be achieved using georeferenced point clouds generated from UAS imagery. In their accuracy

assessments, the point cloud accuracy strayed from DGPS reference measurements by only 2.5-4cm. Similarly, Clark (2017) used UAS imagery to assess coastal change on Prince Edward Island. The author used two types of UAS – fixed-wing and quadcopter – to generate digital elevation models of coastal erosion dynamics to compare their respective accuracies (Clark, 2017). In reference to real-time kinematic (RTK) GPS coastal traces, they achieved average horizontal accuracies of 25cm for the fixed-wing UAS and 21cm for the quadcopter UAS, and average vertical accuracies of 11cm for the fixed-wing UAS and 2.24cm for the quadcopter UAS.

### **1.3 Forested wetlands**

The term forested wetland covers a wide variety of ecosystems globally. However, in the context of this research, it will refer only to forested wetland communities in Nova Scotia. In general, forested wetlands are an understudied and undervalued ecosystem type that are often overlooked in the discourse of wetland conservation (Smith, et al. 2007). For example, in Nova Scotia's Wetland Conservation Policy, the term *forested wetland* is only mentioned twice (The Government of Nova Scotia, 2011). Despite the scarcity of studies related to forested wetlands, they are believed to hold high conservation value relative to other types of forests in Nova Scotia (Brazner and Achenbach, n.d.; Harper et al., 2016). Forested wetlands are ubiquitous across Nova Scotia, but their distribution is not well characterized or well known. Based on Nova Scotia's wetland inventories, Brazner and Achenbach (n.d.) estimate that forested wetlands make up at least 6% of Nova Scotia's land cover – although this estimate is considered to be very conservative, as certain types of forested wetlands are severely under-represented in the inventories.

Forested wetlands hold high levels of biodiversity in both flora and fauna, and provide habitat for some at risk species, especially birds. Westwood (2016) found that three bird species at risk – the Canada Warbler, Rusty Blackbird, and Olive-sided Flycatcher – are known to nest in forested wetland ecosystems. In addition, forested wetlands provide many important ecosystem services, such as recreation and flood storage (Faulkner, 2004). In addition, their biogeochemical processes can retain and transform pollutants, which are effective means of enhancing water quality (Faulkner, 2004, cited in Faulkner 2004).

#### **1.4 Net primary productivity**

NPP is a measurement used to determine the production of biomass by vegetation. It is usually measured in grams of dry weight biomass per square meter per year ( $\text{g}/\text{m}^2/\text{year}$ ) produced both above and below ground less losses to respiration, herbivory, and mortality (Cronk and Fennessy, 2009; Scurlock and Olson, 2002). NPP is a widely used ecosystem variable that is generally more readily available than other biosphere-atmosphere carbon exchange metrics, such as gross primary productivity (GPP) and net ecosystem exchange (NEE; Scurlock and Olson, 2002). The importance of NPP is that it quantifies the availability of plant matter for consumer species (Scurlock and Olson, 2002). Due to its relevance to human interests, NPP studies began in the commercial goods sector, with the monitoring of agricultural and forestry products (Olson, 1964; cited in Scurlock and Olson, 2002). Since then, its use has expanded into a wide range of ecosystem monitoring and assessment applications.

## 1.5 Normalized difference vegetation index

The normalized difference vegetation index (NDVI) is a vegetation index generally used as a proxy measurement for NPP and is calculated using the NIR and red bands of the sensor in use (Equation 1).

Equation 1: Normalized Difference Vegetation Index

$$NDVI = \frac{NIR - Red}{NIR + Red}$$

Adapted from GIS Geography (2018). *What is NDVI (Normalized Difference Vegetation Index)?*

NDVI values range from -1 to 1, with negative values indicating unhealthy or senescent vegetation (or no vegetation), and higher values indicating dense healthy (green) vegetation. NDVI derived from satellite imagery has been used for over two decades to monitor and assess vegetation health at large scales (see Goward et al., 1985). Hobbs et al. (1995) used NDVI derived from the National Oceanographic and Atmospheric Administration's Advanced Very High-Resolution Radiometer satellite imagery set to assess vegetation production in Australia's arid rangelands. From the results, the author determined that NDVI imagery can be used to assess vegetation patterns and productivity in arid regions and can help inform property managers on vegetation-related decisions (Hobbs, 1995). In another early study utilizing NDVI, Ricotta et al. (1999) set out to map and monitor NPP of vegetation using satellite-derived NDVI measurements. The authors compared three cumulative vegetation indices (the integral of NDVI ( $\Sigma$ NDVI), the vectorial representation of NDVI sequential observations in a multidimensional space ( $|$ NDVI) and Fourier analysis (NDVI<sub>S</sub>) to determine if they were equivalent in terms of decision-making (Ricotta et al., 1999). All three indices resulted in the same set of decisions,

indicating that these cumulative indices are statistically equivalent for mapping and monitoring NPP (Ricotta et al., 1999).

Despite the widespread use of NDVI, there are still some concerns with its applicability as a measurement of NPP. Xu et al. (2012) argued that there are significant differences in the spatial and temporal distribution of NPP measurements compared to NDVI measurements. To determine this, the authors used satellite imagery-derived NDVI measurements to compare with NPP field measurements. From the results, Xu et al. (2012) found that NDVI values were correlated with NPP measurements, but the spatial distribution of the two metrics varied to a significant degree. The authors concluded that NPP approximation using NDVI to assess vegetation health can be applicable in some cases, but it depends on the ecological context of the study (Xu et al., 2012). However, this position is held by the minority of researchers, and NDVI is still widely accepted as an approximation of NPP. For example, Goward et al. (1985) determined that NPP patterns matched those of NDVI measurements across North America based on the unique spectral characteristics of vegetation in the red and NIR spectrums.

## **1.6 Land cover classification methods**

Classification of land cover types via remote sensing data is often accomplished through one of two main methodologies: supervised classification, and unsupervised classification. Both involve using computer learning algorithms that group the pixels of a raster layer into categories based on the similarity of their spectral signatures (Peacock, 2014). The key distinction between the two methods is that supervised classification involves user input prior to the algorithm being applied to the dataset, whereas unsupervised classification does not (Peacock, 2014). This input requires a priori knowledge of the land cover types in the study area. This knowledge is often in

the form of field data that are collected prior to the classification, usually referred to as “ground truth data”. These data are collected and recorded with known geographic locations, and thus can be identified in the dataset (G. Baker, personal communication, June 23<sup>rd</sup>, 2018). Once identified, these areas of known land cover are selected as “training polygons” for the algorithm. The algorithm then builds a signature file that is applied to the dataset.

Peacock (2014) recently compared the accuracy of unsupervised and supervised land cover classification methods using LANDSAT imagery in Little Rock, Arkansas. The author used confusion matrices to assess the accuracy of the two methods and found that unsupervised classification led to generally higher classification success. This result contradicts the generally held conception that supervised classification is more accurate than unsupervised classification. However, flaws in training sites and the skill of the user may have played a factor in the result, as higher skill levels are generally required for proper supervised classification. When properly conducted, supervised classification can be more reliable and allows for more control over the grouping of pixels by the user. For example, Weih et al. (n.d.) found that supervised classification outperformed unsupervised classification in accuracy assessments, with an average accuracy of 64.1% for supervised classification versus 60.1% for unsupervised classification.

## **CHAPTER 2: Methods**

### **2. Study area**

The study site was selected from a set of previously sampled forested wetland landscapes in Nova Scotia. Factors taken into account during the selection of the site include: 1) proximity to built-up areas and aerodromes, as Transport Canada regulations state that UAS operation under

the exemption from the Special Flight Operations Certificate must take place at least three nautical miles from any built-up area, and 5 nautical miles from any aerodrome; 2) site accessibility and; 3) amount of forest canopy cover, as ground control points (GCPs) must be placed in areas where they are visible from above.

The study area is located near Musquodoboit Harbour, Nova Scotia, in the Musquodoboit River Valley. The Musquodoboit River Valley runs through Colchester and Halifax Counties, extending approximately 56 km until its terminus at the Atlantic Ocean on the eastern shore of Nova Scotia (Lin, 1970). The site is bordered by Highway 357 to the west, and by the Musquodoboit River to the east (Figure 1). The land cover in the area is a mosaic of different habitat types, including treed bog, alder thicket, shoreline thicket, shoreline meadow, open bog, mixedwood upland forest, spruce-hemlock forest, spruce-pine forest, wet coniferous forest, and wet deciduous forest (The Nature Conservancy of Canada, 2016). The understory vegetation is comprised of a variety of moss species (largely *Sphagnum* species in wet areas); shrubs, such as lambkill (*Kalmia angustifolia*), false holly (*Nemopanthus mucronatus*), and speckled alder (*Alnus incana*); and ferns, including cinnamon fern (*Osmundastrum cinnamomeum*) and eastern bracken fern (*Pteridium aquilinum*).

The site is a protected conservation area owned by the Nature Conservancy of Canada, and represents habitat for several species of concern, such as the Canada Warbler (*Cardellina canadensis*), and black-footed reindeer lichen (*Cladonia stygia*). Despite its protection, there is evidence of use by humans in the form of foot paths and all-terrain vehicle trails that criss-cross through the open areas of the bog. There is also an old logging road (now mostly overgrown) that runs approximately east-west from Highway 357 toward the Musquodoboit River. However, no

significant current anthropogenic uses have been identified (The Nature Conservancy of Canada, 2016). The topography in the area is mostly smooth or flat, which is characteristic of inland bogs, marshes, and swamps in Nova Scotia, and is underlain mostly with organic soils (The Nature Conservancy of Canada, 2016).

## **2.1 Ground control point placement**

GCPs are points on the ground with a known geographic location and are visible in the processed imagery (Clark, 2017). During processing, the coordinates of the GCPs are uploaded into the processing software, and each GCP is identified in the imagery and selected as a reference point. This georeferences the imagery by linking the known location of the GCP to the image. In this case, the GCPs were sheets of plywood painted with a checkerboard pattern. G. Baker (personal communication, June 22, 2018) noted that the checkerboard pattern is best as it allows the centre of the target to be better identified in the imagery than other patterns (e.g. bullseye pattern) if there is any kind of distortion (e.g. if the image is washed out, pixelated, etc.). Prior to any UAS flights, anticipated GCP locations were selected via visual assessment using the free software Google Earth. To ensure that each GCP appeared in a sufficient number of images, GCPs were placed in a “double-X” pattern, and spaced so that no GCP was greater than 6 times the distance of the shortest image edge from any adjacent GCP, and GCPs at the border of the study site were no more than 1.5 times the distance of the shortest image edge from the border of the study site. This rationale was developed through trial and error during previous studies carried out by technicians and researchers at the Maritime

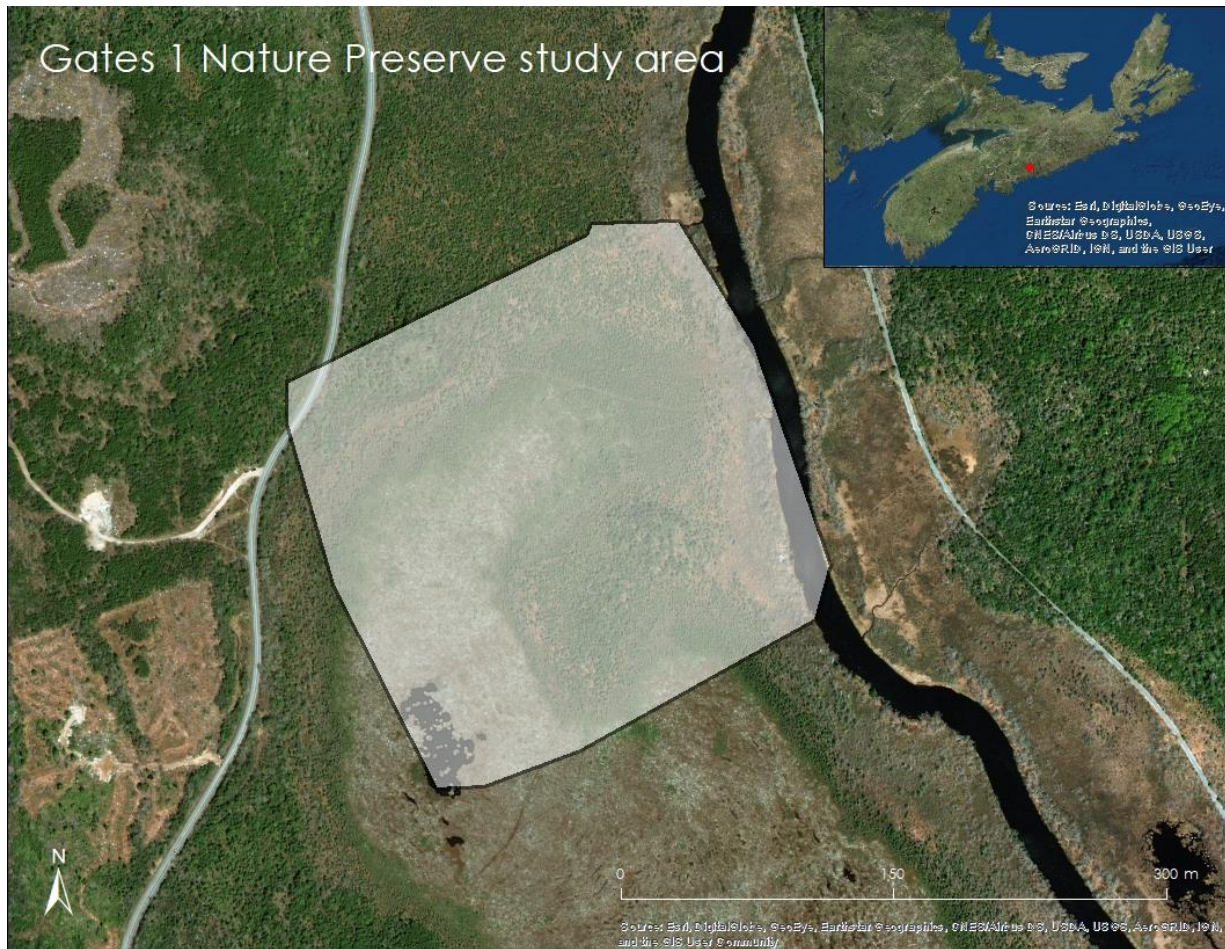


Figure 1: Study area at Gates 1 Nature Preserve. The white shaded area represents the extent of the study area.

Provinces Spatial Analysis Research Centre (MP\_SpARC; G. Baker, personal communication, June 22, 2018). In this case, the shortest edge of any image collected was 35m ground distance at a flying height of 90m (G. Baker, personal communication, June 22, 2018). Thus, each anticipated GCP location was selected such that they would be no more than approximately 210m ( $6 \times 35\text{m} = 210\text{m}$ ) from any adjacent GCP, and that GCPs at the border of the site were no greater than approximately 52.5m ( $1.5 \times 35\text{m} = 52.5\text{m}$ ) from the edge of the study site.

The coordinates of the anticipated GCP locations were inputted into a Garmin GPSMAP 64s handheld GPS (+/- 5m) for use in the field. The high amount of canopy cover and topographical variation within the study site required some adjustment of the location of the GCPs from the anticipated locations that were selected (Figure 2). For example, there may not have been a sufficient break in the forest canopy at the anticipated location, and thus it was required that the GCP be shifted to a nearby area with a canopy break. In addition, there was one significant change in elevation within the study site (a sharply rising hill/outcropping near the middle of the site), and thus a GCP was required at that location to capture all the topographical variation. As the GCPs were placed, the absolute location of the centre of each GCP was surveyed using a Leica GS-14 GNSS RTK Rover at sub-centimetre accuracy.

## **2.2 Ground truth plot point generation**

In order to quantify land cover types, ground truth plots were distributed throughout the study site. To capture the variability in land cover within the study site and to avoid any potential bias in the selection of ground truth plots (e.g. selecting areas with greater ease of access over other harder to access areas), a systematic grid of points was generated using the *Create Fishnet* tool in ArcMap 10.6 GIS software. The study site was broken up into two polygons and the following process was repeated for each polygon. First, a polygon of the study site was uploaded into the ArcMap project and selected as the output feature class for the fishnet. The size of the fishnet grid was then selected as 5x5, and all other settings were left as default. Once the fishnet was generated, the *Clip (Data Management)* tool was used to eliminate all generated points that did not fall within the study area polygons. Due to the orientation of the polygons (i.e. not positioned perfectly north-south), the points were distributed on an angle. This process resulted

in the generation of 14 points in the first polygon, and 13 points in the second polygon for a total of 27 ground truth data collection points (Figure 3). The coordinates of each point were then inputted into a Garmin GPSMAP 64s handheld GPS ( $\pm 5\text{m}$ ) for use in the field.

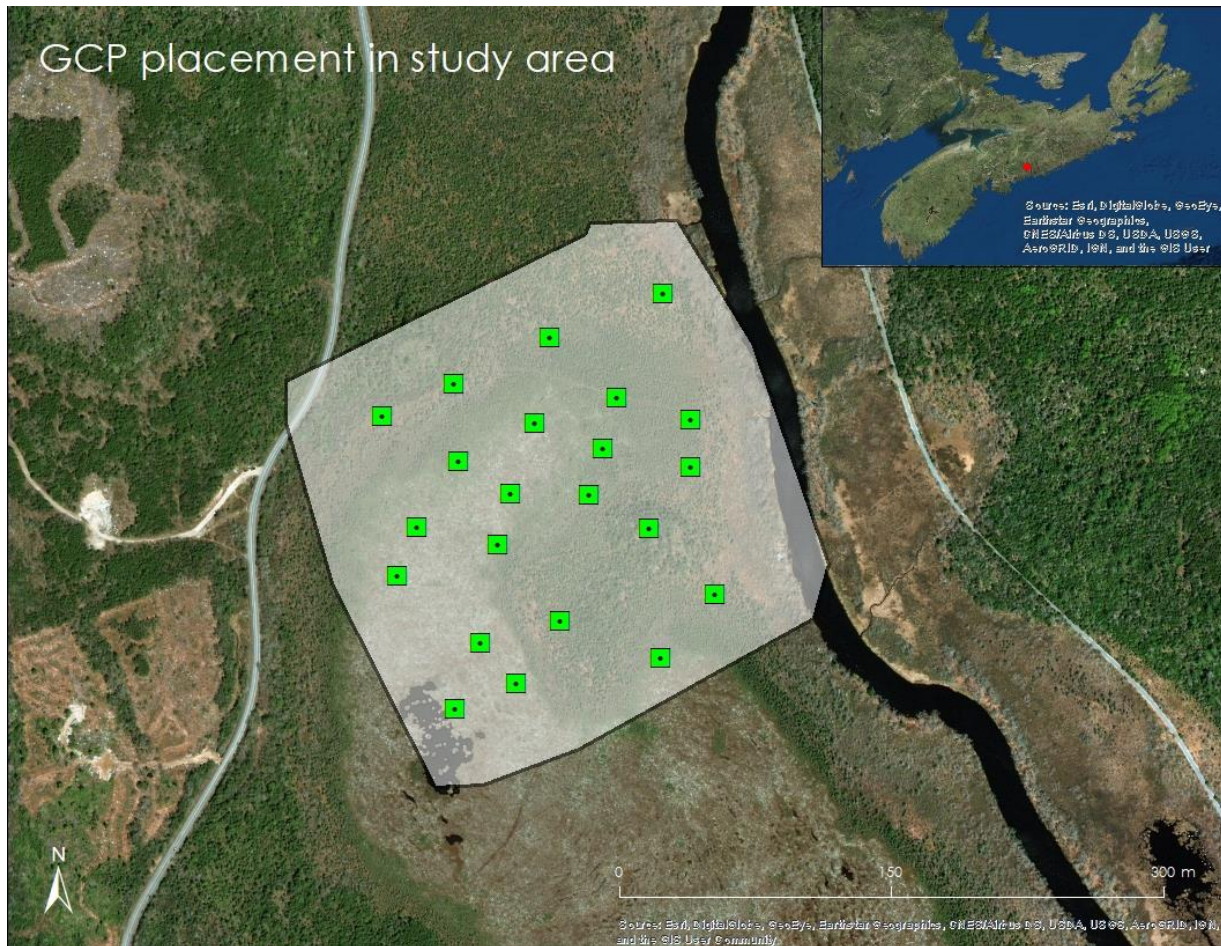


Figure 2: Ground control points at Gates 1 Nature Preserve. Green points represent the location of ground control points.

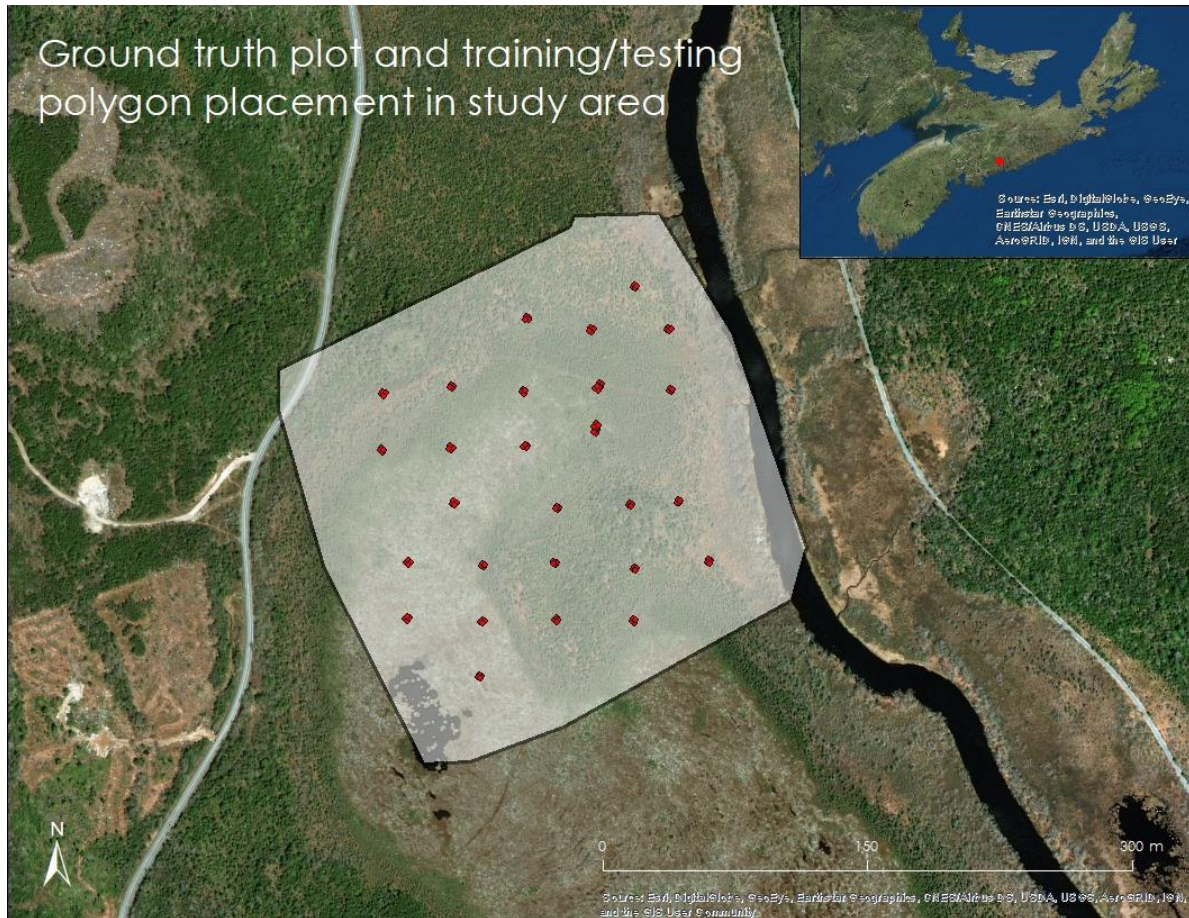


Figure 3: Ground truth plots at Gates 1 Nature Preserve. Red dots represent training polygon locations at the study site.

### 2.2.1 Ground truth plot and sampling design

The ground truth protocol was carried out at each of the ground truth plots. The chosen ground truth data collection method was adapted from Brazner and Achenbach (n.d.). The protocol is largely based upon the Forest Ecosystem Classification guide for Nova Scotia, and the Canadian Wetland Classification System, with some modifications by Brazner and Achenbach (n.d.) to better reflect field observations of forested wetlands and to avoid misclassification due to overly broad vegetation categories (Brazner and Achenbach, n.d.).

As discussed in Brazner and Achenbach (n.d.), there are generally 4 types of forested wetland ecosystems as classified under the CWCS found in Nova Scotia – wooded bogs, wooded fens, wooded swamps, and shrub swamps. However, given the close similarity in vegetation structure between wooded bogs and wooded fens, Brazner and Achenbach deemed it unnecessary to distinguish between them and grouped these two types into one category as *peatlands*. Thus, Brazner and Achenbach (n.d.) used three main classes of forested wetlands in their study: 1) treed swamps; 2) shrub swamps and; 3) peatlands. For the present research, in addition to the wetland classes described by Brazner and Achenbach (n.d.), any area that was clearly not a wetland area (i.e. had unsaturated soil, 0cm peat depth) was classified simply as forested upland. Table 1 below shows the criteria for each land cover class.

Table 1: Land cover class criteria.

<u>Class</u>	<u>Criteria</u>
Peatland	<30% cover in tree layer and >40cm peat depth
Shrubbed swamp	>30% cover in high shrub layer and <30% cover in tree layer
Treed swamp	>=30% cover in tree layer
Treed upland	Any forested area with 0cm peat depth and relatively dry soil (i.e. unsaturated)

The first step of the protocol outlined in Brazner and Achenbach (n.d.) consists of delineating a circular plot with a 30m radius from a central point and completing a rapid visual survey of the area to estimate the cover of six distinct vegetation strata: 1) moss layer; 2) fern

layer; 3) herbaceous layer; 4) low shrub layer (woody vegetation <2m in height); 5) high shrub layer (woody vegetation 2-7m in height) and; 6) tree layer (woody vegetation >7m in height). Due to time constraints for this project and the relatively large amount of points that were to be sampled (in contrast, Brazner and Achenbach (n.d.) only sampled one point per wetland), the radius of the plot was reduced to 15m. The second step of the protocol was to dig a soil pit and measure peat depth to determine if the area is considered a peatland. Each of these steps was carried out at each of the 27 ground truth points.

### **2.2.2 Training polygon delineation**

Once the ground truth data had been collected, training polygons to be used in the supervised classification were delineated within each of the 15m radius plots. To do this, a 5x5m square was created by taking four compass bearings at 0°, 90°, 180°, and 270°, measuring 2.5m from the centre of the ground truth plot in each of the four directions, and placing a survey flag. These flags served as the vertices for the training polygon, and the location of each vertex was recorded using a Leica GS-14 GNSS RTK Rover. Some areas selected for ground truth data collection had higher land cover variability than others, and so multiple polygons were surveyed within the 15m radius plot at some of the points to better capture the land cover characteristics at these points.

### **2.3 UAS imagery capture**

Aerial imagery was captured using a DJI Phantom 4 Pro off-the shelf, consumer grade quadcopter. The full system consisted of the quadcopter, imagery payload, and two-way link controller. The relevant imagery payload equipped to the quadcopter consisted of a 1.2-

megapixel Sentera Single-NDVI sensor mounted on a fixed nadir gimbal. The Sentera sensor captures imagery at two very specific bands in the electromagnetic spectrum: the red band at 625nm centre wavelength with a 100nm bandwidth, and the near-infrared (NIR) at 850nm centre wavelength with a 40nm bandwidth (Sentera, 2017). This imagery is then converted into NDVI imagery in post-processing.

Pix4D Capture – a free UAS flight mapping software that can be downloaded onto any smartphone operating on Android or iOS – was used to map flight plans prior to flights and autonomously control the UAS during flights. Fraser and Congalton (2018) found that a flying height of 100m above the canopy was ideal for forested environments. However, due to restrictions on flying height for pilots operating under the exemption from the Special Flight Operations Certificate, the flying height was set to 90m. Conversely, lower flying heights would result in higher battery usage and lower image alignment success (Fraser and Congalton, 2018). Image overlap for the Sentera Single-NDVI sensor had to be set manually through the firmware installed on the SD card that is inserted into the sensor. Various options for image overlap settings exist within the firmware, such as GPS Distance trigger, GPS Time trigger, and GPS Overlap trigger (Sentera, 2017). Given that the GPS onboard the sensor only has an accuracy of +/- 5m, the GPS Time trigger option was selected in an effort to maintain the greatest possible accuracy of image capture during the flights. To achieve 80% overlap for proper orthomosaic stitching, the maximum speed of the quadcopter during its grid-pattern flights and the image ground footprint size of the Sentera Single-NDVI sensor were identified. In this case, the maximum speed of the quadcopter during the grid-pattern flights at 90m flying height was approximately 5m/s, and the image ground footprint of the sensor was 104x35 m at a flying

height of 90m. Therefore, to attain 80% overlap, the amount of time between each shutter trigger was set to 1.4 s.

One set of two flights was completed on July 13<sup>th</sup>, 2018, and the second was completed on August 24<sup>th</sup>, 2018. Calibration images were captured before and after each flight using an Airinov radiometric calibration target. This calibration process allows for images from different flights, days, and sites to be comparable to one another, which is especially important for multi-spectral imagery (G. Baker, personal communication June 26, 2018). Reflectance values of the Airinov radiometric calibration target for the bandwidths at which the Sentera Single NDVI sensor. Prior to going into the field, an Ocean Optics USB 2000 spectrometer was used to measure the reflectance values of the target across a wide range of the electromagnetic spectrum. From these results, the reflectance values were identified for the bandwidths of the Sentera Single NDVI sensor.

## **2.4 Image pre-processing**

The imagery was uploaded into the Pix4D Mapper Pro imagery processing software suite to undergo orthomosaic stitching via a Structure-from-Motion Multi-View Stereopsis (SfM-MVS) workflow. SfM-MVS is a workflow technique to derive georeferenced densified 3D point clouds from 2D imagery. It is distinct from typical photogrammetry – the science of deriving reliable spatial measurements from aerial imagery (Khorram et al., 2012) – in that many of its aspects stem from advances in 3D computer vision algorithms, rather than advances in photogrammetry itself (Smith et al., 2016). Another key distinction between SfM-MVS and traditional photogrammetry is that much of the SfM-MVS workflow is automated, including the computation of the camera orientation and position, and internal camera geometry, which

requires manual inputs from the user in traditional photogrammetry techniques (Micheletti et al., 2015). However, it should be noted that many photogrammetric philosophies and methods are embedded in SfM-MVS workflows (Micheletti et al., 2015). A wide variety of means of achieving the end goal of SfM-MVS exist, although the general concept remains constant across all methods. At the core, multiple views of an object are captured using a digital camera from multiple positions (Micheletti et al., 2015). Common features in the images are then identified by computer algorithms in sufficient detail to define their spatial relationships in an arbitrary 3D coordinate system (Micheletti et al., 2015). From these spatial relationships, a sparse 3D point cloud is created. The sparse point cloud is then densified using MVS techniques.

Since NDVI is a time dependent index, the following process was carried out for both sets of imagery from flight days 1 and 2 separately. Steps 1 and 2 of the Pix4D Mapper Pro processing workflow were run to generate key points and point clouds. The GCP coordinates were then entered in the GCP/MTP Manager, and the GCP coordinates were manually confirmed using the GCP Editor. Next, the final processing step was run to densify the point cloud and generate the initial orthomosaic and digital surface models.

Once the initial orthomosaics and digital surface models were generated, the Index Calculator in Pix4D Mapper Pro was used to generate reflectance maps. Reflectance values (expressed in values between 0 and 1 to represent percentages from 0% to 100%) for the red band and the NIR band were entered into the calculator and the final processing step was re-run to generate the reflectance maps.

## 2.5 Image post-processing

The completed reflectance maps were uploaded into ArcMap 10.6 to generate NDVI maps. The Sentera Single NDVI sensor is a modified RGB sensor which results in some “bleed-over” between the red and NIR channels (Sentera, 2017). Thus, a raster calculation was performed to isolate the red and NIR bands, compensate for unequal irradiance between the red and NIR bands, and compute NDVI values. Equation 2 is a reduction of several formulas that accomplish these tasks (see Sentera, 2017).

Equation 2: Calculating NDVI from original pixel digital number

$$NDVI = \frac{(1.236 \times DN_{ch3}) - (0.188 \times DN_{ch1})}{(1 \times DN_{ch3}) + (0.044 \times DN_{ch1})}$$

Adapted from: Sentera. (2017). *False color to NDVI conversion: precision NDVI single sensor*.

Technical document received via email.

The calculation was input into the *Raster Calculator* tool in ArcMap10.6 with the reflectance maps as the raster input.

### 2.5.1 Image classification

To perform the land cover classification, the training polygon vertex coordinates were uploaded into ArcMap 10.6 and the *Image Classification* toolbar was enabled. The NDVI rasters for flight days 1 and 2 were also uploaded. Once again, these steps were performed separately for flight days 1 and 2. The raster was selected in the toolbar as the subject of analysis, and polygons were drawn using the training polygon vertex points as reference. The polygons were then merged into their corresponding classes based on the ground truth data (peatland, shrubbed

swamp, treed swamp, or treed upland). Polygons were also drawn over the known non-consequential land cover types – open water and the small amount of paved road in the western part of the day 1 map – to account for all types of cover in the scene. Approximately half of the polygons were used as training data to generate the signature file, while the other half were saved for testing data for the accuracy assessment. The signature file was generated using the training data, and the *Maximum Likelihood Classification* tool was run using the NDVI raster as the input to generate the land cover classification raster. The maximum likelihood algorithm functions by assuming a normal distribution among the pixel values in each band. It then compares the pixel values of the classes within the signature file with those of the unclassified pixels in the dataset, and groups them based on the means and covariances of the unclassified pixels (ESRI, 2018).

### **2.5.2 Image classification accuracy assessment**

To assess the accuracy of the classification system, the imagery underwent a series of steps to generate quantitative values of accuracy. The *Create Accuracy Assessment Points* tool generates random points within a feature and creates a table with two columns – GROUND\_TRUTH and CLASSIFIED – which are populated with the corresponding class values of the generated points. The user may select this first step to be either ground truth data or classified data. In this case, the ground truth points were created first so that the classified points would be generated within the test site polygons, rather than distributed throughout the entire study area. The tool was run with the test data polygons as the input to populate the GROUND\_TRUTH field of the table. The number of points was set to 1600, and the sampling strategy was selected as equalized stratified random so that the same number of points would be generated within each class. Next, the *Update Accuracy Assessment Points* tool was run using

the generalized classified raster as the input raster and the output of the *Create Accuracy Assessment Points* tool as the input table. With both fields populated, the final table was used as the input for the *Compute Confusion Matrix* tool and a confusion matrix was generated.

### **2.5.3 Imagery generalization**

To improve the visual appearance of the NDVI maps after the accuracy assessment, the following series of steps were undertaken to filter, smooth, and generalize the imagery: 1) the *Majority Filter* tool was run to remove single isolated pixels; 2) the *Boundary Clean* tool was run to clump regions and smooth ragged edges; 3) the *Region Group* tool was run to assign unique values to each region in the image with a lower threshold of 300 pixels selected to identify unnecessary small areas; 4) a mask was created to remove these small areas using the *Set Null* tool to set the small areas of  $\leq 300$  pixels to a null pixel value; and 5) the *Nibble* tool was run on the land cover classification raster with the mask raster from the previous step as the input mask raster to dissolve the small regions from the image.

### **2.5.4 NDVI value assessment**

The secondary objective for this project was to assess the NDVI values (i.e. productivity) within each class. To accomplish this, the completed classification raster was transformed into a polygon using the *Raster to Polygon* tool in ArcMap. The *Create multipart features* box was checked to ensure that only a single multipart polygon was created for each class, rather than several small polygons representing each region of classified pixels. Each of these multipart polygons was then exported to its own feature class. The road and water classes were left out of this process because the NDVI values of these classes were irrelevant. These separated polygons

were then used as the inputs for the zonal data in the *Zonal Statistics* tool which was run on each class. The original pre-classification NDVI raster was used as the input value raster, and the zone field was selected as the object ID of the polygon.

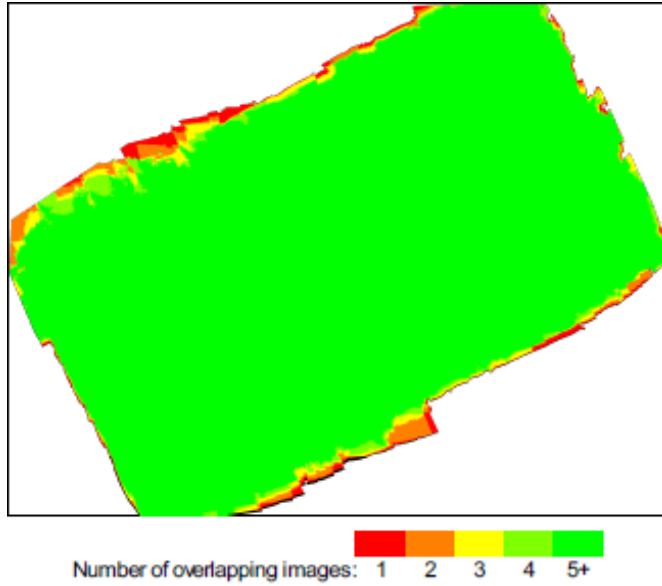
## CHAPTER 3: Results

### 3. Results

The ground truth surveys yielded some initial insight into the proportion of land cover at the site. Based on the classification scheme adapted from Brazner and Achenbach (n.d.), the most abundant land cover surveyed was the shrubbed swamp class, which accounted for approximately 44% of the surveyed plots. The next most abundant land cover classes were peatland (30%) and treed swamp (22%). Treed upland accounted for the least amount of land cover, with only approximately 4%. These proportions were in congruence with general field observations during sampling.

Overall, the quality reports generated by Pix4D Mapper Pro indicated that the orthomosaic generation was successful with a sufficient number of overlapping images for flight days 1 and 2 (Figure 4). However, 2D key point matches between individual images were low in many areas for flight days 1 and 2 (Figure 5). Generally, these low match areas corresponded to areas of denser forest cover. Ground cell distance (i.e. resolution) was reported to be 7.90cm for flight day 1, and 8.05cm for flight day 2.

(a)



(b)

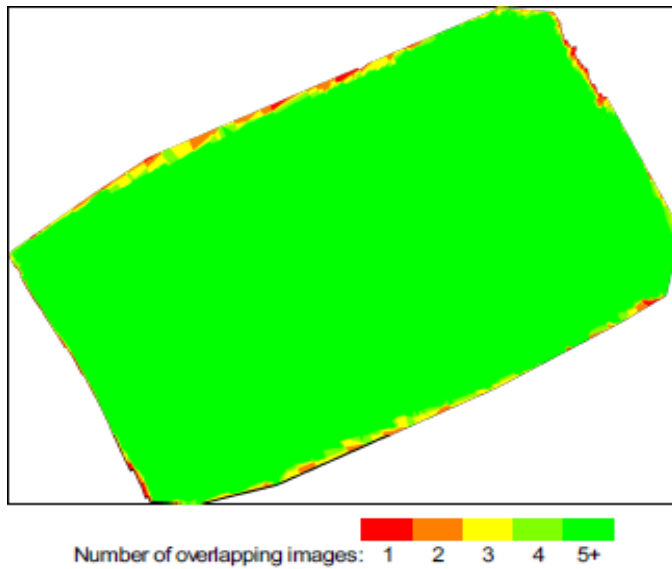
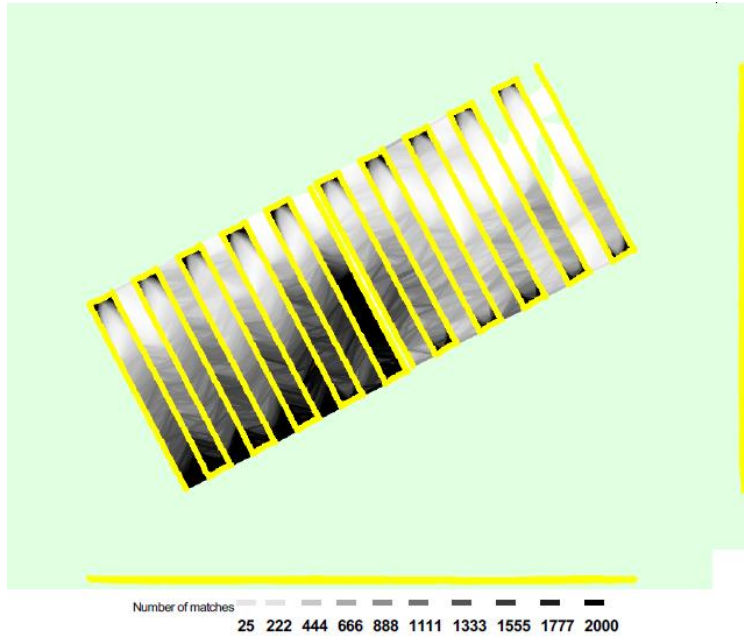


Figure 4: Number of overlapping images computed for each pixel of the orthomosaic for flight day 1 (a) and flight day 2 (b). Red and yellow areas indicate low overlap for which poor results may be generated. Green areas indicate an overlap of over 5 images for every pixel.

(a)



(b)

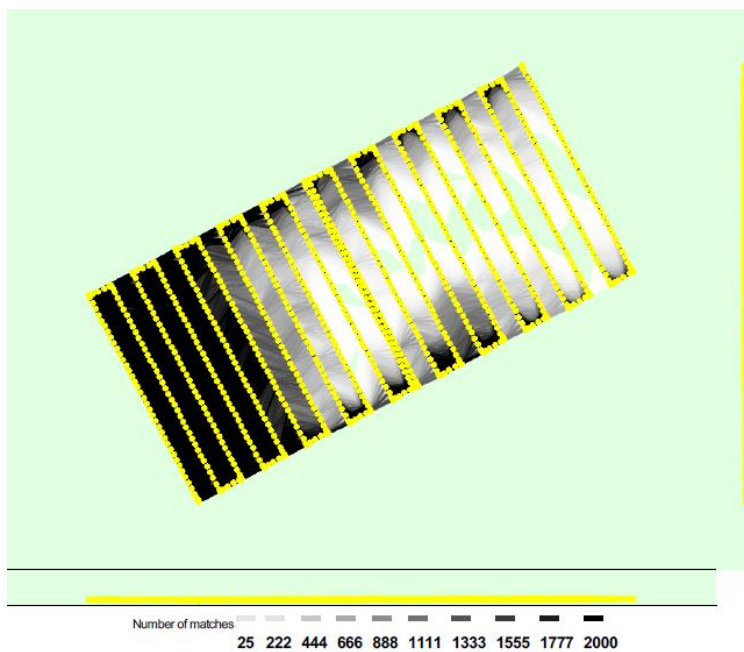
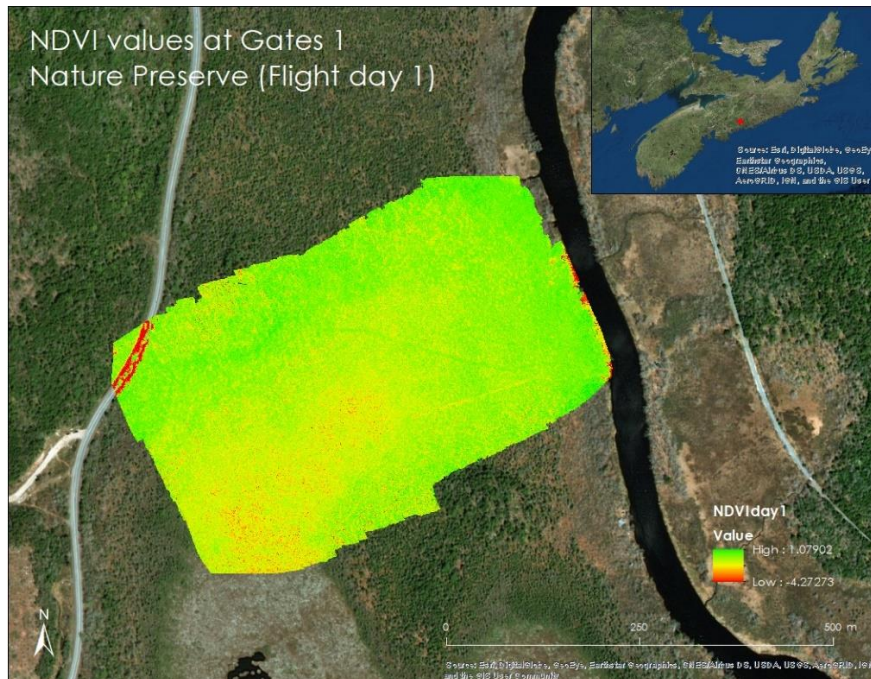


Figure 5: Computed image positions with links between matched images for flight day 1 (a) and flight day 2 (b). Dark areas indicate a high number of links between images, and bright areas indicate low numbers of links between images.

The initial NDVI maps (Figure 6) showed NDVI values that extended beyond the range of the scale (max of 1.07 and min of -4.27 for day 1, and a min of -4.27 for day 2). Upon closer examination of the data, there were virtually no pixels with these erroneous values present in the image and were thus deemed outliers due to processing error. Visually, the NDVI values appeared very similar across the study area (i.e. monochromatic), which was backed up by the NDVI value assessment. The mean NDVI values from day 1 were fairly similar between classes, ranging from 0.76 in the shrubbed swamp class, to 0.82 in the treed swamp class (Figure 7). The mean NDVI values from day 2 were also quite similar, ranging from 0.79 in the peatland class to 0.84 in the treed upland class (Figure 7).

The classification map of flight day 1 (Figure 8) indicates the dominance of the treed swamp class (dark green), with smaller areas of peatland (brown) and shrubbed swamp (light green) in the first half of the site. The small amounts of paved road and open water in the imagery appear to be confused by the classification algorithm. The classification map of flight day 2 (Figure 8) indicates the dominance of the peatland and treed upland class throughout the other half of the site, with some treed swamp and virtually no shrubbed swamp present. The water in the day two map is correctly classified, aside from distortion in the far right of the image, likely due to warping and stretching during the Pix4D processing stage.

(a)



(b)

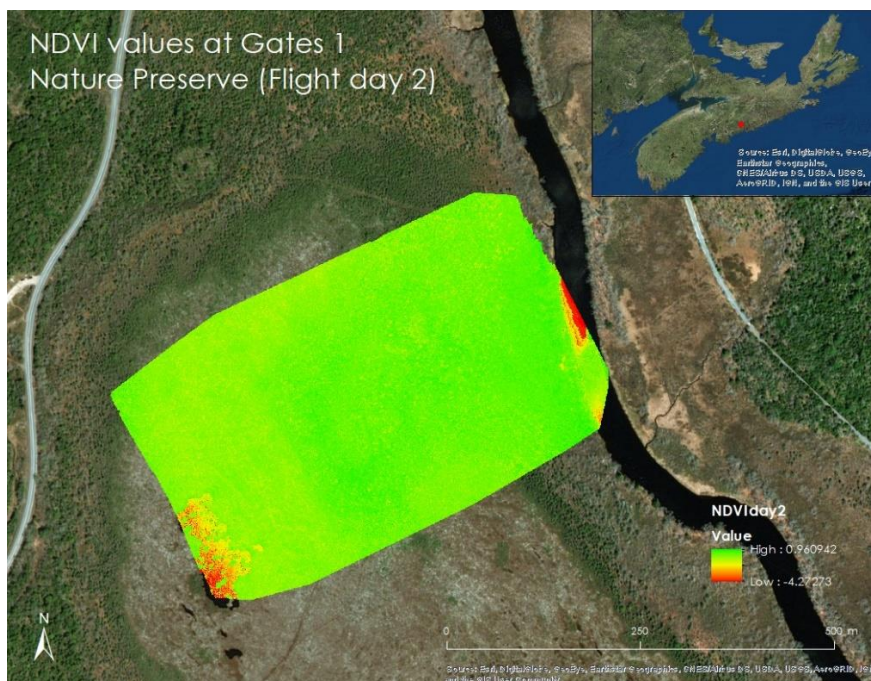
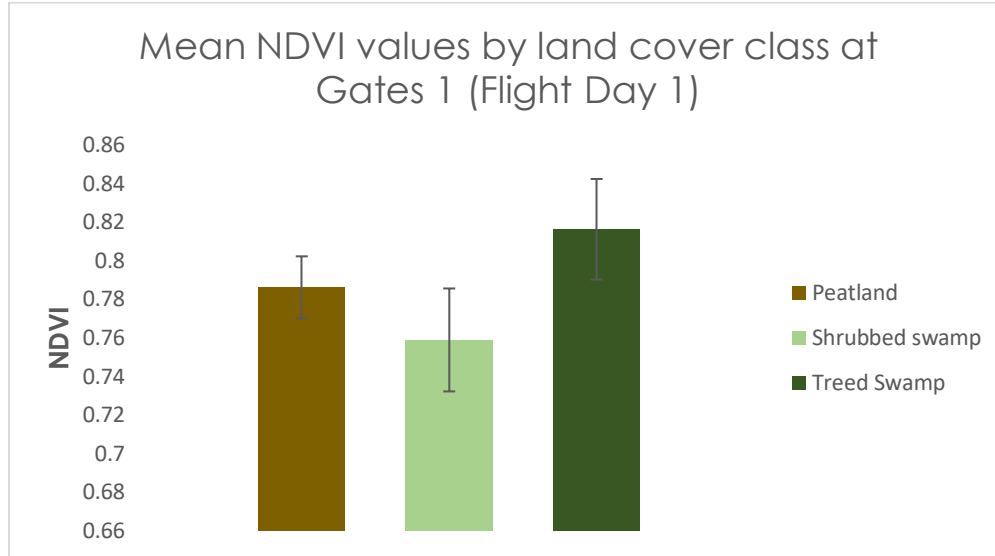


Figure 6: NDVI values from flight day 1 (a) and flight day 2 (b) at Gates 1 Nature Preserve.

(a)



(b)

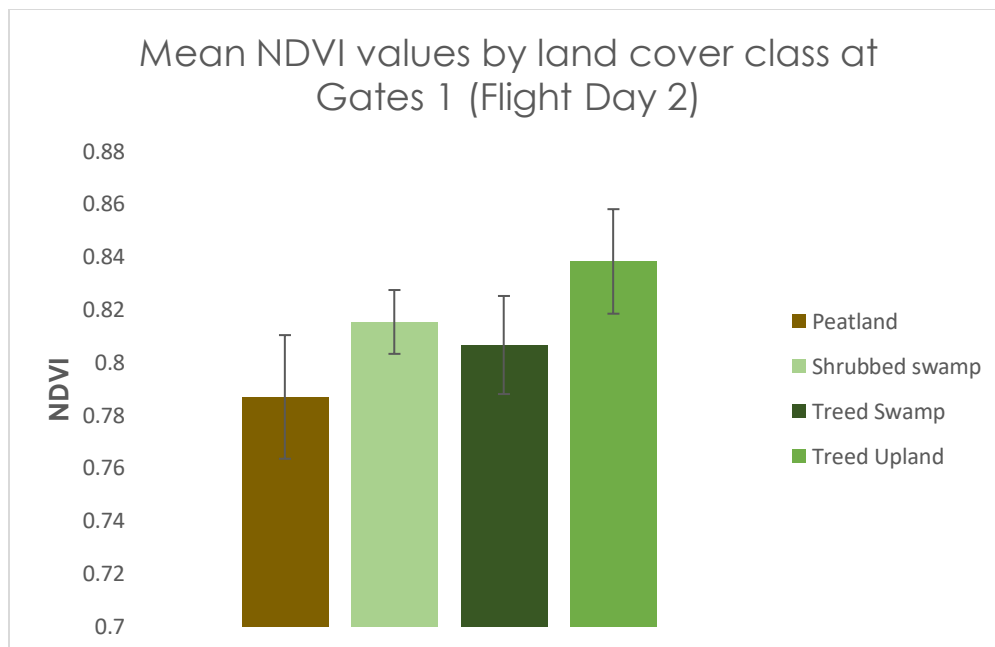
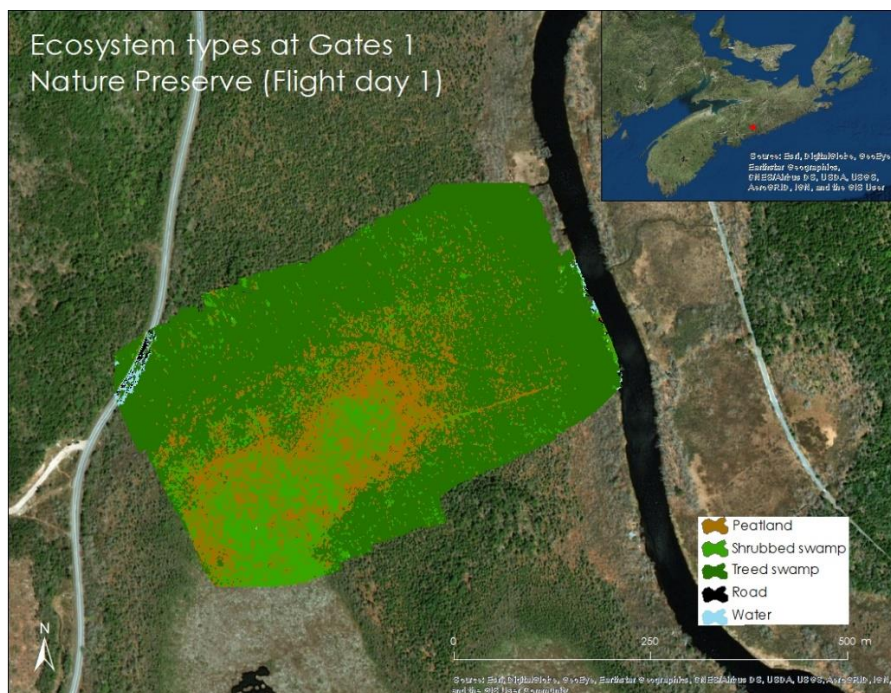


Figure 7: Mean NDVI values from flight day 1 (a) and flight day 2 (b) with standard deviation.

(a)



(b)

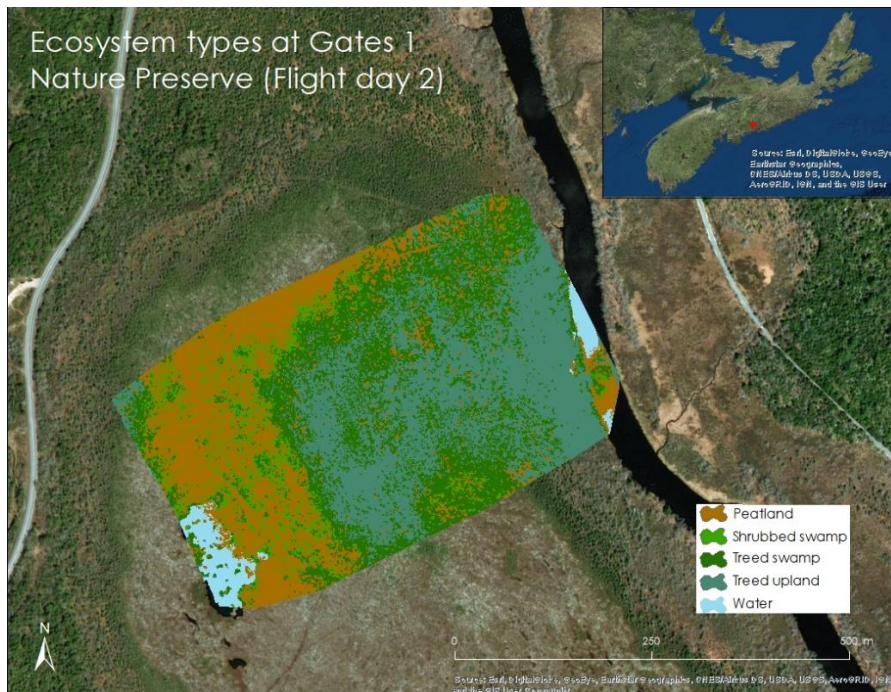


Figure 8: Classification of ecosystems from flight day 1 (a) and flight day 2 (b) at Gates 1 Nature Preserve.

Confusion matrices are a means of assessing the accuracy of a supervised classification. They examine if a given pixel was correctly classified based on a predicted result, and provide a percentage of success of the classification, known as the kappa coefficient. In the matrix, rows represent *user accuracy*, while the columns represent *producer accuracy*. User accuracy is a measure of error by commission – otherwise described as a false positive. These false positives are pixels that are classified as one class, while they should have been classified as another based on the classification scheme. It indicates the probability of the pixel representing the actual land cover (Jensen, 2005). Producer accuracy is a measure of error by omission, or false negatives. It indicates how accurately reference pixels were classified (Jensen, 2005). The kappa coefficient measures how well the classified map matches the ground truth data (Jensen, 2005). It takes into account both chance success and overall accuracy.

The confusion matrix for flight day 1 (Table 2) indicates user accuracies between 0.13 (shrubbed swamp class) and 0.90 (road class), and producer accuracies between 0.076875 (shrubbed swamp class) and 0.96 (water class). The confusion matrix for flight day 2 (Table 3) indicates user accuracies between 0.27 (shrubbed swamp class) and 0.99 (water class), and producer accuracies between 0.14 (shrubbed swamp class) and 1 (water class).

Table 2: Confusion matrix for flight day 1.

<b>Class</b>	<b>Peatland</b>	<b>Shrubbed swamp</b>	<b>Treed swamp</b>	<b>Road</b>	<b>Water</b>	<b>Total</b>	<b>User Accuracy</b>	<b>Kappa</b>
<b>Peatland</b>	684	471	519	0	0	1674	0.41	0
<b>Shrubbed swamp</b>	577	123	223	27	8	958	0.13	0
<b>Treed swamp</b>	293	990	856	0	0	2139	0.40	0
<b>Road</b>	10	3	1	666	58	738	0.90	0
<b>Water</b>	36	13	1	907	1534	2491	0.62	0
<b>Total</b>	1600	1600	1600	1600	1600	8000	0.00	0
<b>Producer Accuracy</b>	0.43	0.08	0.54	0.42	0.96	0.00	0.48	0.00
<b>Kappa</b>	0	0	0	0	0	0	0.00	0.35

Table 3: Confusion matrix for flight day 2.

<b>Class</b>	<b>Peatland</b>	<b>Shrubbed swamp</b>	<b>Treed swamp</b>	<b>Treed upland</b>	<b>Water</b>	<b>Total</b>	<b>User Accuracy</b>	<b>Kappa</b>
<b>Peatland</b>	1102	226	55	15	0	1398	0.79	0
<b>Shrubbed swamp</b>	336	216	223	29	0	804	0.27	0
<b>Treed swamp</b>	152	474	640	193	0	1459	0.44	0
<b>Treed upland</b>	0	684	682	1363	0	2729	0.50	0
<b>Water</b>	10	0	0	0	1600	1610	0.99	0
<b>Total</b>	1600	1600	1600	1600	1600	8000	0.00	0
<b>Producer Accuracy</b>	0.69	0.14	0.40	0.85	1.00	0.00	0.62	0.00
<b>Kappa</b>	0	0	0	0	0	0	0.00	0.52

## CHAPTER 4: Discussion and recommendations

### 4. Image classification

The classification was far less than satisfactory. The Kappa values of 0.35 and 0.52 for flight days 1 and 2, respectively, are well below the desired accuracy (0.9+). Even when simply visually examining the classified imagery, there are evident errors. Based on field observations and ground truth data, there was far more of the shrubbed swamp class than any other class present at the site. However, almost no pixels of this class value appear in the imagery from either flight day. In addition, both the user and producer accuracy in the confusion matrices

indicate that the shrubbed swamp class was a large source of error. The producer and user accuracies for the treed swamp class are also low, which indicates that these two classes are likely being confused for one another during the classification, leading to false land cover information. Field observations also indicated that these two classes often shared plant species and were sometimes very similar in structural make-up. In addition, the ground truthing protocol that was employed relied almost solely on subjective assessments of vegetation cover, which could have led to misclassification on the ground, further confounding the imagery classification.

Training polygon delineation was also potentially problematic for pixel-based classification methods. To ensure proper signature file generation, training polygons should be comprised of homogenous cover across their extent (G. Baker, personal communication, June 22, 2018). During sampling, it was not ensured that the cover contained within the vertexes of the polygon was homogenous, but simply that the polygon was within a zone of known cover. The polygons were within an area of a known land cover class based on the ground truth protocol (e.g. shrubbed swamp), but at times contained several different plant species and other aspects of ground cover – both within the same polygon (e.g. a polygon with both maple and alder), and between different classes of polygons (e.g. a polygon with all maple trees within it was classified as a shrubbed swamp, and a polygon with all alder individuals was also classified as a shrubbed swamp). If more ground truth samples had been taken to account for this variation within and between polygons, errors might have been minimized. However, with only a small sample of ground cover, these errors were amplified.

The similarity in NDVI values in the maps used for the classification likely also contributed to the poor performance of the classification. The Maximum Likelihood Classification algorithm operates based on differences in pixel values of each band in the image. If the distribution of

digital numbers within a band does not fit the assumed normal distribution, the algorithm places these pixels into different classes (ESRI, 2018). Thus, if the digital numbers of the bands are very similar (as they are in this case), the algorithm may not properly assign each pixel.

#### **4.1 NDVI value assessment**

NDVI values were similar across all classes from both flight days, with a range of approximately 0.08. This is peculiar, as it was expected that the open area of the peatland would have much lower productivity than the forested areas of the wetland. While this could be a significant result (i.e. productivity does not greatly differ between forested and unforested wetlands), the poor quality of the classification suggests that these values may not hold much meaning. This may be due to issues with the equipment used, and the pre- and post-processing techniques employed during the study. The sensor employed for this study was not designed for use with the Pix4D Mapper Pro software suite, and consequently required some “Jerry-rigging” to derive a functional workflow. Particularly, the raster transformation formula provided by Sentra may not have accounted for the calibration that takes place during the Pix4D Mapper Pro reflectance map generation process. Since the calibration was applied before the raster transformation formula, the NDVI values may be erroneous. In addition, SfM-MVS techniques are not well-suited to the forested landscape, as the structure of a forest canopy is too complex to construct an accurate orthomosaic from aerial imagery (G. Baker, personal communication, June 22<sup>nd</sup>, 2018). The complexity across the surface of the tree canopy makes it difficult for the software to compute enough unique key points to create a high-quality image.

Mean NDVI values were also much higher than expected. Generally, high NDVI values (0.6-0.8) are seen in areas of highly productive vegetation, such as tropical rainforest (NASA,

2000). The mean NDVI values found during this study (approximately 0.75-0.83) do not align with the expected values for a temperate bog ecosystem with moderate productivity. White et al. (2016) found NDVI values in wetlands in Australia ranging between 0.11 and 0.8. This indicates that there are possible issues with some part of the NDVI calculations in the workflow of this study. However, NDVI is a highly time-dependant variable that can change greatly over the course of a few days or weeks (C. Ross, personal communication, February 25, 2019), and at the height of the growing season it is not unlikely for a highly productive wetland to display these values. More imagery from different sites is required to determine if these NDVI values are truly erroneous.

#### **4.2 UAS effectiveness in forested wetland landscapes**

Based on the results produced during this study, this particular methodology was not effective in classifying this specific forested wetland landscape. Overall, the orthomosaic generation was successful. However, areas of dense forest cover appeared to reduce the quality of the orthomosaic, indicated by the low number of 2D key point matches. The complex nature of forest canopy structure tends to make SfM-MVS-based orthomosaic stitching challenging (G. Baker, personal communication, June 26<sup>th</sup>, 2018). Fraser and Congalton (2018) recently investigated aspects of UAS data collection in forested landscapes that contribute to spatial accuracy and output quality. In the data collection stage, the authors tested three different heights for UAS flights above the forest canopy: 50m; 100m; and 120m (Fraser and Congalton, 2018). In the processing stage, two software suites were tested for output quality and accuracy: Pix4D Mapper Pro; and Agisoft Photoscan. The results showed that the 100m flying height led to improved photo alignment success, higher average number of tie points per image, and ideal

planimetric model ground sampling distance compared to other flying heights (Fraser and Congalton, 2018). In addition, Agisoft Photoscan was found to be superior in its output quality to that of Pix4D Mapper Pro with 11.8% greater image alignment success and a 9.91% finer planimetric model resolution (Fraser and Congalton, 2018). Based on these findings, future attempts to classify forested wetlands could benefit from a higher flight height and the use of Agisoft Photoscan, instead of Pix4D Mapper Pro. However, for the present study, Pix4D Mapper Pro was the only photogrammetry software available for use, and flying height was restricted by Transport Canada regulations surrounding UAS use.

Further, overall classification performance was poor, and various technical issues added up to a less-than-efficient workflow. NDVI values were successfully assessed across the various classes of land cover, although the high level of confusion across classes indicates that these values are essentially meaningless. In terms of comparable studies, there are very few examples of remote sensing being applied in forested wetlands, and fewer examples of UAS use – possibly due to the complex structure and ephemeral nature of forested wetlands. However, some relevant instances exist. Wang (2018) recently used UAS imagery in conjunction with historical air photographs and point pattern analysis to determine the extent of tree encroachment in bogs in Nova Scotia. While the focus of the study was not UAS imagery, the author employed UAS in a novel approach to analyzing forested wetland communities (Wang, 2018). In addition, there are some relevant examples of UAS use in drier forested environments that have led to some success. Dandois and Ellis (2013) used UAS to map and assess forest canopy structure and spectral dynamics in 3D. The authors carried out a study that employed off-the-shelf UAS equipped with a standard digital camera to collect data on forest structure and spectral attributes. The goal of the research was to develop a methodology that could assess forest canopy dynamics

over the course of a growing season (Dandois and Ellis, 2013). This required repeated flights over the study area to collect the temporal dynamics of both the canopy height and canopy spectral characteristics. The results showed that UAS imagery measurements were highly correlated with satellite NDVI measurements ( $R^2 = 0.87$ ), demonstrating strong evidence that this novel methodology can capture vegetation structural and spectral phenological dynamics at the spatial scale of individual trees, which was an important breakthrough in terms of forest ecology (Dandois and Ellis, 2013).

Separate from UAS-based approaches, satellite-based remote sensing has also been applied to forested wetlands. Townsend and Walsh (2001) utilized multispectral and multitemporal satellite imagery to determine plant community structure and composition in forested wetlands in the southeastern USA. The authors developed a hierarchical classification scheme using imagery collected by the Landsat Thematic Mapper in different parts of the growing season (March-April, May-June, and July-August) so as to take advantage of phenological differences in forest community structure (Townsend and Walsh, 2001). Interestingly, the study employed an unsupervised ISODATA classification approach to iteratively classify different land covers as opposed to supervised classification methods, which are more widely used. The process began at the broad scale, and eventually narrowed the classification down to the single-species level (Townsend and Walsh, 2001). The result was a highly accurate classification method for forested wetlands backed up by field surveys. Townsend and Walsh (2001) provide a novel means of classifying forested landscapes through unsupervised classification, which seems to go against the grain of most ecological classification studies that employ supervised classification methods.

### 4.3 Recommendations for future direction

For future attempts to use UAS in forested wetlands, there are several recommendations for increasing success. One large source of error during the supervised classification was the similarity between the shrubbed and treed areas (both wetland and upland) in terms of their spectral signatures. Pixel-based classification methods rely solely upon the differentiation between these spectral signatures. Therefore, these methods are much better suited to areas with greater homogeneity *within* land cover types, and greater differentiation *between* land

cover types. Furthermore, pixel-based methods may be better applied to large-scale imagery (e.g. air photos and satellite imagery) of forested wetlands with lower resolutions. While high-resolution imagery is generally desirable as it provides greater levels of detail, at lower resolutions, land covers will appear generally more homogenous across their extents, leading to better differentiation between classes. In addition, pixel-based methods do not take into account textures, shapes, or heights of objects within the study area. Thus, much of the nuance that is present in high-resolution imagery is not utilized to its full extent (e.g. canopy crowns of trees). Other types of image classifications exist that may be better suited to high-resolution remotely-sensed imagery of forested wetlands, such as object-based image analysis (OBIA) techniques. In general, pixel-based classification methods highlight noise, create a salt-and-pepper effect, and ignore important topological and contextual information in imagery (Pande-Chhetri et al., 2017). In contrast, OBIA methods use shapes in conjunction with spectral characteristics to classify imagery, which takes into account many of these aspects in addition to spectral information. Pande-Chhetri et al. (2017) recently compared OBIA classification techniques to pixel-based methods for classifying freshwater wetlands in Florida, USA, using high-resolution (8cm) UAS imagery. To achieve optimal performance in the classification, the authors also compared three

separate classification algorithms applied to each classification method (OBIA and pixel-based): 1) support vector machine; 2) artificial neural network; and 3) maximum likelihood (Pande-Chhetri et al., 2017). From the results, it was determined that OBIA methodologies using the support vector machine algorithm outperformed other algorithms within the OBIA methods, and all pixel-based methods with an overall accuracy of 70.8%. This study indicates that OBIA methods may greatly improve the performance of the classification of forested wetlands.

Future attempts would also likely benefit from a multivariate analysis approach that incorporated canopy heights into the classification. Much of the confusion between classes resulted from similarities in spectral signatures. Thus, it can be concluded that vegetation in this particular location had similar productivity (i.e. NDVI values; assuming NDVI values are correct) across classes; however, field observations indicate that vegetation in the shrubbed swamp and treed swamp classes was much taller than in the open peatland areas. Therefore, if the vegetation height had been included as part of the classification, classes could have been distinguished more reliably.

The ground truth protocol may have also been a source of error, resulting in flaws in the classification. The protocol was designed based on subjective assessments of vegetation ground cover in various strata which added up to an ecosystem description (e.g. peatland, shrubbed swamp, treed swamp). This likely resulted in high variability of spectral signatures within classes and high similarity between classes, contributing to the poor performance of the classification. Supervised classification methods often make use of vegetation species-based ground sampling to delineate homogenous areas or groups of single species, as opposed to the general land cover-based approach used in this study. In this case, a species-based ground sampling approach would not have been practical. High species diversity at the site would have made it extremely

impractical given the time-frame allotted, and thus the general land cover-based approach made the most sense for this project. However, to increase the performance of the classification, a more rigorous and quantitative approach to land cover ground sampling is recommended for future attempts. For example, the Forest Ecosystem Classification (FEC) system that was developed for Nova Scotia uses a much more robust system of classifying ecosystem types based on a variety of aspects, including soil type, vegetation cover type, and moisture level (Neily et al., 2011). This system or an adaptation of this system may be better suited to this type of project.

#### **4.4 Conclusion**

Overall, this project was unsuccessful in achieving its objectives of classifying a forested wetland landscape and assessing productivity within it. However, the general concept of classifying forested wetlands through remote sensing is sound and could help to improve forested wetland inventorying and mapping. Having a good understanding of the spatial distribution of sensitive ecosystems is crucial in management and conservation decision-making. Without accurate maps and inventories, these ecosystems may suffer due to anthropogenic impacts, such as logging and development. Thus, improving our understanding of forested wetlands through remote sensing methods could help conserve and maintain important habitat and ecosystem services.

## LIST OF REFERENCES

Brazner, J., and Achenbach, L. (n.d.). *Breeding bird assemblages associated with forested wetlands from three ecoregions in western Nova Scotia: Does conservation value differ among site types?* Unpublished research project with the Department of Natural Resources.

Clark, A. (2017). Small unmanned aerial systems comparative analysis for the application to coastal erosion monitoring. *GeoResJ*, 13, 175-185.

Cronk, J.K., and Fennessy, M.S. (2009). Wetland plants: the primary productivity of wetland plants. In G.E. Likens (Ed.), *Encyclopedia of Inland Waters* (pp. 590-598). Amsterdam, Netherlands: Elsevier.

Dandois, J., and Ellis, E. (2013). High spatial resolution three-dimensional mapping of vegetation spectral dynamics using computer vision. *Remote Sensing of Environment*, 136(C), 259-276.

ESRI. (2018). *How Maximum Likelihood Classification works*. Retrieved from <http://desktop.arcgis.com/en/arcmap/latest/tools/spatial-analyst-toolbox/how-maximum-likelihood-classification-works.htm> Accessed on February 24, 2019

Fraser, B. T., and Congalton, R. G. (2018). Issues in Unmanned Aerial Systems (UAS) Data Collection of Complex Forest Environments. *Remote Sensing*, 10(6).

The Government of Nova Scotia (2011). *Nova Scotia's Wetland Conservation Policy*. Retrieved from <https://novascotia.ca/nse/wetland/docs/Nova.Scotia.Wetland.Conservation.Policy.pdf> Accessed on November 17, 2018.

GIS Geography (2018). *What is NDVI (Normalized Difference Vegetation Index)?* Retrieved from <https://gisgeography.com/ndvi-normalized-difference-vegetation-index/> Accessed on April 25<sup>th</sup>, 2018.

Goward, S., Tucker, N., and Dye, C. (1985). North American vegetation patterns observed with the NOAA-7 advanced very high resolution radiometer. *Vegetatio*, 64(1), 3-14.

Harper, K. (2016). *Biodiversity and ecosystem functioning of forested wetlands across Atlantic Canada*. Unpublished project description for application of funding to the Atlantic Ecosystem Initiative.

Hobbs, T. (1995). The use of NOAA-AVHRR NDVI data to assess herbage production in the arid rangelands of Central Australia. *International Journal of Remote Sensing*, 16(7), 1289-1302.

Jensen, J. R. (2005). *Introductory Digital Image Processing: A Remote Sensing Perspective (3rd ed.)*. Upper Saddle River, NJ: Pearson.

Khorram, S. (2012). *Remote sensing* (SpringerBriefs in space development). New York: Springer.

Kuželka, K., and Surový, P. (2018). Mapping Forest Structure Using UAS inside Flight Capabilities. *Sensors*, 18(7).

Lin, C. (1970). The Hydrogeology of the Musquodoboit River Valley. Nova Scotia Department of Mines: Groundwater Section Report 70-3.

Lucieer, A., and Harwin, S. (2012). Assessing the Accuracy of Georeferenced Point Clouds Produced via Multi-View Stereopsis from Unmanned Aerial Vehicle (UAV) Imagery. *Remote Sensing*, 4(6), 1573-1599.

Micheletti N., Chandler J.H. and Lane. S.N. (2015) Section 2.2. Structure from Motion (SfM) photogrammetry. In: Cook SJ, Clarke LE and Nield JM (eds) *Geomorphological Techniques* (Online Edition). London, UK: British Society for Geomorphology. ISSN: 2047-0371.

Michez, A., Piégay, H., Jonathan, L., Claessens, H., and Lejeune, P. (2016a). Mapping of riparian invasive species with supervised classification of Unmanned Aerial System (UAS) imagery. *International Journal of Applied Earth Observations and Geoinformation*, 44(C), 88-94.

Michez, A., Piégay, H., Lisein, J., Claessens, H., and Lejeune, P. (2016b). Classification of riparian forest species and health condition using multi-temporal and hyperspatial imagery from unmanned aerial system. *Environmental Monitoring and Assessment*, 188(3), 1-19.

The Nature Conservancy of Canada. (2016) *Gates 1 Property: Musquodoboit River PMP – Eastern Shore Forest and Coast NA: Baseline Inventory*. Unpublished ecosystem inventory report.

NASA. (2000). *Measuring vegetation (NDVI & EVI)*. Retrieved from <https://earthobservatory.nasa.gov/features/MeasuringVegetation> Accessed on February 25, 2019

Neily, P., Basquill, S., Quigley, E., Stewart, B., and Keys, K. (2011). Forest Ecosystem Classification for Nova Scotia. *Nova Scotia Department of Natural Resources Renewable Resources Branch*.

Pande-Chhetri, R., Abd-Elrahman, A., Liu, T., Morton, J., and Wilhelm, V. (2017). Object-based classification of wetland vegetation using very high-resolution unmanned air system imagery. *European Journal of Remote Sensing*, 50(1), 564-576.

Peacock, R. (2014). *Accuracy Assessment of Supervised and Unsupervised Classification using Landsat Imagery of Little Rock, Arkansas* (Master's thesis). North West Missouri State University, Maryville, Missouri.

Puliti, S., Ørka, H. O., Gobakken, T., and Næsset, E. (2015). Inventory of small forest areas using an unmanned aerial system. *Remote Sensing*, 7(8), 9632-9654.

Ricotta, C., Avena, G., and De Palma, A. (1999). Mapping and monitoring net primary productivity with AVHRR NDVI time-series: Statistical equivalence of cumulative vegetation indices. *ISPRS Journal of Photogrammetry and Remote Sensing*, 54(5), 325-331.

Sentera. (2017). *False color to NDVI conversion: precision NDVI single sensor*. Technical document received via email.

Scurlock, J., and Olson, R. (2002). Terrestrial net primary productivity a brief history and a new worldwide database. *Environmental Reviews*, 10, 91-109.

Smith, C., Morissette, J., Forest, S., Falk, D., and Butterworth, E. (2007). Synthesis of technical information on forest Wetlands in Canada. NCASI Technical Bulletin. 1-97

Smith, M., Carrivick, J., and Quincey, D. (2016). Structure from motion photogrammetry in physical geography. *Progress in Physical Geography*, 40(2), 247-275.

Townsend, P., and Walsh, A. (2001). Remote sensing of forested wetlands: Application of multitemporal and multispectral satellite imagery to determine plant community composition and structure in southeastern USA. *Plant Ecology*, 157(2), 129-149.

Wang, R. (2018). *A multi-method assessment of the temporal dynamics of treed bogs in Nova Scotia, Canada* (Master's thesis). Dalhousie University, Halifax, NS.

Weih, R. C. Jr., and Riggan, N. D. Jr. (n.d.). Object-Based Classification vs Pixel-Based Classification: Comparative Importance of Multi-Resolution Imagery. *The International Archives of the Photogrammetry, Remote Sensing and Spatial Information Sciences*, Vol. XXXVIII-4/C7.

Westwood, A. (2016). *Conservation of three forest landbird species at risk: Characterizing and modelling habitat at multiple scales to guide management planning*. (Unpublished PhD dissertation). Dalhousie University, Halifax, NS.

White, D., Lewis, M., Green, G., and Gotch, T. (2016). A generalizable NDVI-based wetland delineation indicator for remote monitoring of groundwater flows in the Australian Great Artesian Basin. *Ecological Indicators*, 60(C), 1309-1320.

Xu, C., Li, Y., Hu, J., Yang, X., Sheng, S., and Liu, M. (2012). Evaluating the difference between the normalized difference vegetation index and net primary productivity as the indicators of vegetation vigor assessment at landscape scale. *Environmental Monitoring and Assessment*, 184(3), 1275-1286.

## APPENDIX

Site: Musq.				Date: 08/08/2018 - 09/08/2018				
GT point	Mos s	Fer n	Her b	Shrub <2	Shrub 2-7	Tre e	Peat dpth	Result:
1	80	0	20	70	1	0	40+	Peatland
2	80	0	10	70	20	1	40+	Peatland
3	100	0	20	60	30	20	29	Shrubbed swamp
4	100	60	30	50	50	10	35	Shrubbed swamp
5	100	20	40	40	50	20	40+	Shrubbed swamp
6	80	0	20	70	1	0	40+	Peatland
7	80	0	20	70	40	10	40+	Shrubbed swamp
8	70	10	20	80	30	5	40+	Shrubbed swamp
9	70	0	10	70	50	20	24	Shrubbed swamp
10	80	0	10	70	20	5	40+	Peatland
11	60	30	10	40	10	40	22	Treed swamp
12	100	0	10	40	30	30	40+	Treed swamp
13	100	50	20	10	60	40	40+	Treed swamp
14	100	90	10	5	10	30	40+	Treed swamp
15	80	0	5	50	0	0	40+	Peatland
16	80	0	5	50	0	0	40+	Peatland
17	80	0	5	70	40	10	40+	Shrubbed swamp
18	80	0	5	50	0	0	40+	Peatland

19	90	0	5	50	0	0	40+	Peatland
20	100	60	30	30	20	40	35	Treed swamp
21	90	60	20	30	30	50	20	Treed swamp
22	100	0	5	70	40	20	40+	Shrubbed swamp
23	100	0	0	5	5	50	0	Treed upland
24	100	40	5	5	30	10	40+	Shrubbed swamp
25	90	5	10	60	40	5	40+	Shrubbed swamp
26	100	70	10	10	60	10	40+	Shrubbed swamp
27	90	80	5	10	40	10	40+	Shrubbed swamp

Figure A 1: Ground truth plot vegetation data.

(a)

**Summary**

Project	MJSQ_NDM
Processed	2018-09-18 19:36:09
Camera Model Name(s)	NIR_1.2MP-GS-0002_4.14mm-0001_0006_4.1_1248x950 (RGB)
Average Ground Sampling Distance (GSD)	7.90 cm / 3.11 in
Area Covered	0.199 km <sup>2</sup> / 19.8654 ha / 0.08 sq. mi. / 49.1140 acres
Time for Initial Processing (without report)	03h:39m:44s

**Quality Check**

<b>Images</b>	median of 21520 keypoints per image	
<b>Dataset</b>	1844 out of 1844 images calibrated (100%), all images enabled	
<b>Camera Optimization</b>	0.49% relative difference between initial and optimized internal camera parameters	
<b>Matching</b>	median of 10387.9 matches per calibrated image	
<b>Georeferencing</b>	yes, 11 GCPs (11 3D), mean RMS error = 0.046 m	

**Preview**

(b)

**Summary**

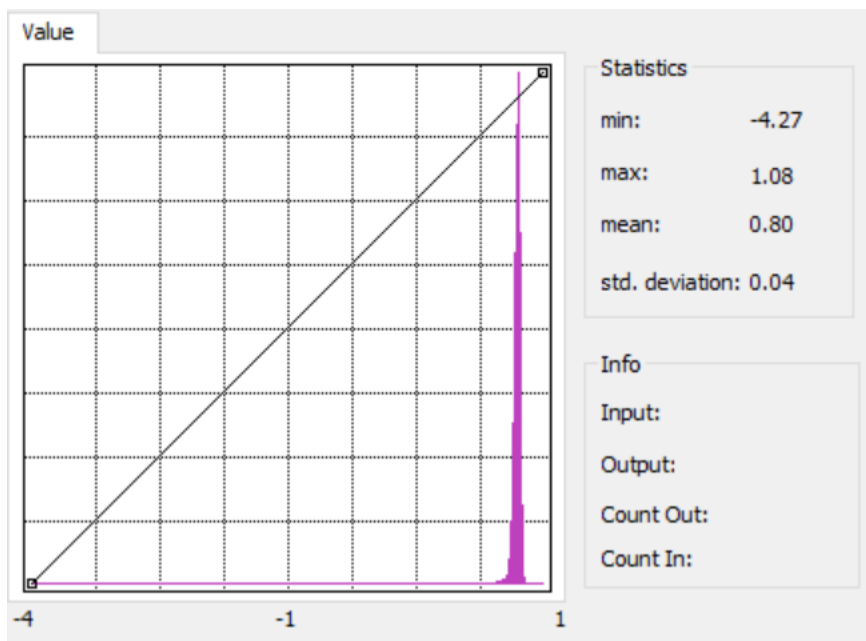
Project	MJSQ_NDM_D2
Processed	2018-09-19 20:33:40
Camera Model Name(s)	NIR_1.2MP-GS-0002_4.14mm-0001_0006_4.1_1248x950 (RGB)
Average Ground Sampling Distance (GSD)	8.05 cm / 3.17 in
Area Covered	0.203 km <sup>2</sup> / 20.2680 ha / 0.08 sq. mi. / 50.1586 acres
Time for Initial Processing (without report)	01h:30m:50s

**Quality Check**

<b>Images</b>	median of 21413 keypoints per image	
<b>Dataset</b>	1056 out of 1056 images calibrated (100%), all images enabled	
<b>Camera Optimization</b>	0.01% relative difference between initial and optimized internal camera parameters	
<b>Matching</b>	median of 9625.05 matches per calibrated image	
<b>Georeferencing</b>	yes, 11 GCPs (11 3D), mean RMS error = 0.019 m	

Figure A 2: Pix4D Mapper Pro quality report summary for flight day 1 (a) and flight day 2 (b).

(a)



(b)

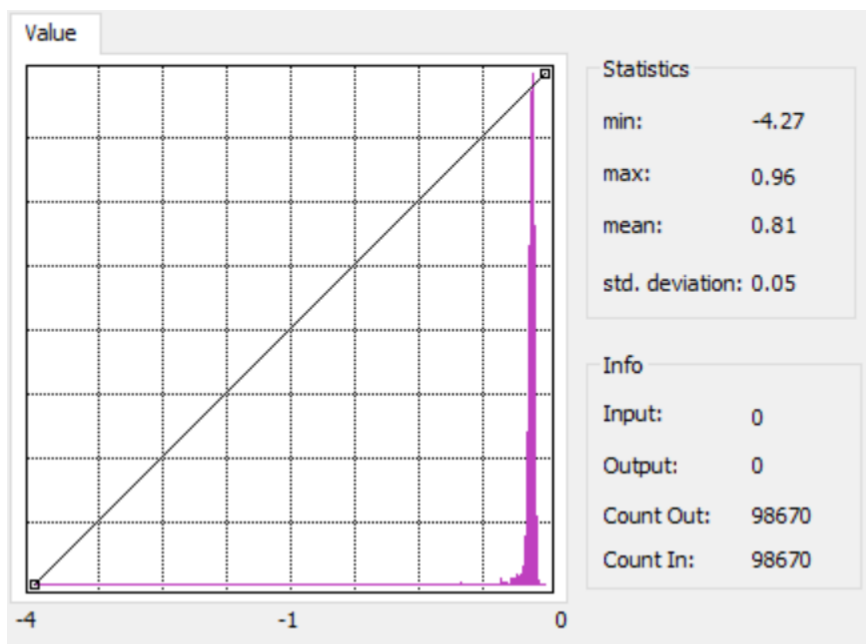


Figure A 3: Pixel value histograms for NDVI maps from flight day 1 (a) and flight day 2 (b).